Journal of Membrane Science 759 (2026) 126150

Contents lists available at ScienceDirect

Journal of Membrane Science

journal homepage: www.elsevier.com/locate/memsci

Supercritical ethylene processing of ZIF-8 membranes towards practical electronic-grade propylene production

Wenjing Hu [a], Pengxiang Zhang [a], Hua Jin [b,c], Jiahui Yan [d], Yuanchen Li [a], Kunpeng Yu [a], Weichong Wang [a], Jiaxin Ma [a], Yumei Meng [a], Weijun Xu [a], Kelin Dong [d,*], Yanshuo Li [b,c,**], Yi Liu [a,***]

[a] State Key Laboratory of Fine Chemicals, Frontiers Science Center for Smart Materials, School of Chemical Engineering, Dalian University of Technology, Dalian, 116024, China
[b] School of Materials Science and Chemical Engineering, Ningbo University, Ningbo, 315211, China
[c] Yongjiang laboratory, Ningbo, Zhejiang, 315202, China
[d] Dalian West Pacific Petrochemical Co., Ltd., Dalian, 116600, China

ARTICLE INFO

Keywords:
ZIF-8 membrane
Supercritical ethylene
C_3H_6/C_3H_8 separation
Microstructure regulation
Electronic-grade C_3H_6

ABSTRACT

ZIF-8 membranes exhibit great promise for high-efficiency C_3H_6/C_3H_8 separation. Nevertheless, maintaining superior performance from pressurized C_3H_6-rich feed streams remains a significant challenge, considering its specific application scenarios (e.g., electronic-grade C_3H_6 production). In this work, we innovatively utilize supercritical ethylene (scC_2H_4) as medium to synthesize ZIF-8 membranes capable of tolerating pressurized high-C_3H_6-ratio feed under sub-freezing temperature. Owing to a wider supercritical operation window of scC_2H_4, both nucleation and growth kinetics of ZIF-8 crystallites can be readily optimized over a broad temperature and pressure range; through combing with moderate reversible π-coordination between unique C═C double bond of scC_2H_4 and Zn^{2+} ions during membrane processing, an unprecedented platform for microstructure optimization of ZIF-8 membranes was established. The introduction of zinc nitrate hydroxide-based buffer layer prior to scC_2H_4 processing further contributed to their superior performance. Under practical electronic-grade C_3H_6 production conditions (i.e., −40 °C, 3 bar, polymer-grade C_3H_6 feed, and vacuum on the permeate side), our membrane achieved C_3H_6/C_3H_8 selectivity of 169.5 with C_3H_6 flux of 3.6×10^{-3} mol m^{-2} s^{-1}, allowing efficient removal of C_3H_6 content from 2998 ppm down to below 50 ppm, which completely fulfilled the purity requirement of electronic-grade C_3H_6 (>99.99%). Through combining with unique advantages of supercritical processing featuring zero waste emission and complete ligand recycling, our research paves an avenue for eco-friendly fabrication of various MOF membranes with tailored microstructures to achieve outstanding separation performance under practical operation conditions.

1. Introduction

Propylene (C_3H_6) is a fundamental chemical feedstock primarily produced via naphtha steam cracking, catalytic cracking, and coal/methanol-to-olefin routes, with propane (C_3H_8) as the major impurity [1–3]. While polymer-grade C_3H_6 (PG C_3H_6, ~99.5%) demands routine C_3H_6/C_3H_8 separation, electronic-grade propylene (EG C_3H_6, purity ≥99.99%, C_3H_8 ≤ 80 ppm) imposes more stringent purification requirements. As an essential carbon precursor for amorphous carbon hard masks in advanced lithography for semiconductors, ultra-deep removal of C_3H_8 impurities has become indispensable [4–8]. Repetitive cryogenic distillation, which is widely employed in trace C_3H_8 removal during EG C_3H_6 production, commonly operates at sub-freezing temperature (~-40 °C) and high pressure (~3 bar) with >100 theoretical trays [9–12], causing significant energy input and capital cost [13–15]. Therefore, it has become imperative to develop an alternative technique for high-efficiency trace C_3H_6 removal in EG C_3H_6 production.

As an energy-efficient and compact alternative to distillation,

* Corresponding author.
** Corresponding author. School of Materials Science and Chemical Engineering, Ningbo University, Ningbo, 315211, China.
*** Corresponding author.
E-mail addresses: dongkl@petrochina.com.cn (K. Dong), liyanshuo@nbu.edu.cn (Y. Li), diligenliu@dlut.edu.cn (Y. Liu).

https://doi.org/10.1016/j.memsci.2026.126150
Received 3 August 2026; Received in revised form 5 September 2026; Accepted 10 September 2026
Available online 11 September 2026
0376-7388/© 2026 Elsevier B.V. All rights are reserved, including those for text and data mining, AI training, and similar technologies.

membrane technique stands out as an attractive strategy for high-efficiency separation, relying on molecular sieving and preferential adsorption mechanisms. Among them, ZIF-8 has been regarded as a promising candidate for precise C_3H_6/C_3H_8 discrimination, considering its appropriate pore aperture (4.0-4.2 Å), which just falls between kinetic diameters of C_3H_6 (4.0 Å) and C_3H_8 (4.2 Å) [16,17]. To date, ZIF-8 membranes have achieved C_3H_6/C_3H_8 separation performance far beyond other membranes [18–20]. In spite of remarkable progress achieved, in most cases their gas permeation properties are measured under ambient conditions. In terms of industrial scenarios for EG C_3H_6 purification under extreme operation conditions (i.e., −40 °C, 3 bar, PG C_3H_6 feed, and vacuum on the permeate side), rare studies have been conducted to explore their potential applications [21–23]. This bottleneck mainly arises from the presence of non-selective grain boundary defects within the membrane [24]. Under above operation conditions, non-selective permeation via intercrystalline gaps is non-negligible, thus inducing inferior C_3H_6/C_3H_8 selectivity [24,25]. Several strategies, including sub-freezing synthesis, interfacial microfluidic synthesis, intergranular bridging reinforcement, vapor-phase synthesis, semi-solid processing, guest molecule confinement, polymer post-modification, dip-coating thermal conversion, as well as supercritical fluid (SCF) processing, have been explored to fabricate pressure-resistant ZIF-8 membranes [26–35]. Nevertheless, relevant research regarding the preparation of ZIF-8 membranes capable of single-step separation for EG C_3H_6 from PG C_3H_6 under practical operation condition remains scarce. Very recently, we pioneered sub-freezing preparation of ZIF-8 membranes toward single-step refinement of PG C_3H_6 into EG C_3H_6 [16]. To realize scalable industrial EG C_3H_6 production, however, developing sustainable route to further enhance the gas permeance with no compromise in EG C_3H_8 purity is urgently required.

Among above methods, supercritical fluids (SCFs) have been proven to be ideal candidate for preparing microstructure-optimized MOF membranes, owing to their unique advantages in terms of zero surface tension, low viscosity, and tunable solubility [36–41]. In terms of C_3H_6-permselective ZIF-8 membranes, employing supercritical CO_2 ($scCO_2$) solvent has been proven competent for synthesizing ZIF-8 membranes possessing outstanding C_3H_6/C_3H_8 selectivity [42], while further using supercritical C_2H_6 (scC_2H_6) solvent enabled the fabrication of pressure-resistant ZIF-8 membranes [35]. Aiming at practical EG C_3H_6 purification, however, not only qualified C_3H_6 purity but also higher C_3H_6 permeance should be achieved. In this regard, selecting new SCF solvent with a broader temperature and pressure range represents a promising solution to address the above issue.

Compared with scC_2H_6 and $scCO_2$ with critical temperatures above 30 °C, the critical temperature of supercritical ethylene (scC_2H_4) was much lower (9.2 °C), enabling modulation of the membrane microstructure over a broader temperature range [43,44]; through combining with the C═C bond in scC_2H_4, which enables mild reversible π-complexation with Zn^{2+} ions, nucleation and growth dynamics of ZIF-8 crystallites could be precisely modulated, facilitating elimination of grain boundary defects, and therefore, formation of pressure-resistant ZIF-8 membranes [45–47].

In this work, we first adopt scC_2H_4 as the reaction medium to fabricate ZIF-8 membranes targeting EG C_3H_6 purification (Fig. 1). Through combining with unique physicochemical properties of scC_2H_4 and dual functions of $Zn_5(NO_3)_2OH_8$ (ZNNH) NSs buffer layer, precise regulation of membrane microstructure could be achieved. Gas permeation results demonstrate that operation pressure exerts limited influence on its C_3H_6/C_3H_8 separation performance; simultaneously, both C_3H_6 permeance and C_3H_6/C_3H_8 selectivity increase with increasing C_3H_6 feed ratio, revealing strong adaptability to practical EG C_3H_6 production. Under realistic industrial conditions, its selectivity reached 169.5 with an ultrahigh C_3H_6 flux of 3.6×10^{-3} mol m^{-2} s^{-1}. Furthermore, vacuum permeation tests were performed with PG C_3H_6 feedstock at −40 °C and 3 bar to simulate industrial heavy impurity removal. Experimental results confirm that as-prepared membrane enables high-efficiency upgrading of PG C_3H_6 to EG C_3H_6 in one step; simultaneously, 2-mIm ligands can be easily recovered from scC_2H_4 via depressurization, thus indicating overall process sustainability.

2. Experimental section

2.1. Reagents and materials

Zinc acetate ($Zn(CH_3COO)_2$, 99.0%) and zinc oxide (ZnO, 99.0%) were supplied by Shanghai Macklin Biochemical Co., Ltd. 2-methoxyethanol ($CH_3OCH_2CH_2OH$, 99.0%) and ethanolamine ($NH_2CH_2CH_2OH$, 99.0%) were obtained from Shanghai Aladdin Biochemical Technology Co., Ltd. Zinc nitrate hexahydrate ($Zn(NO_3)_2{\cdot}6H_2O$, 99.0%) and n-heptane (98%) were provided by Sinopharm Chemical Reagent Co., Ltd. Lithium hydroxide monohydrate ($LiOH{\cdot}H_2O$, ≥98%) was purchased from Sigma-Aldrich. 2-methylimidazole (2-mIm, 98%) was supplied by Shanghai Macklin Biochemical Co., Ltd. Polydimethylsiloxane (PDMS) was obtained from GE Toshiba Silicones Co., Ltd. Methanol (CH_4O, 99.5%) was provided by Tianjin Kemiou Chemical Reagent Co., Ltd. All the above chemicals were employed as received without additional purification. Asymmetric porous α-Al_2O_3 discs (diameter: 18 mm, thickness: 1 mm, pore size: 70 nm) were acquired from Fraunhofer IKTS. H_2 (99.999%), He (99.999%), CO_2 (99.999%), N_2 (99.999%), CH_4 (99.999%), C_3H_6 (99.5%), C_3H_8 (99.5%) and C_2H_4 (99.9%) were

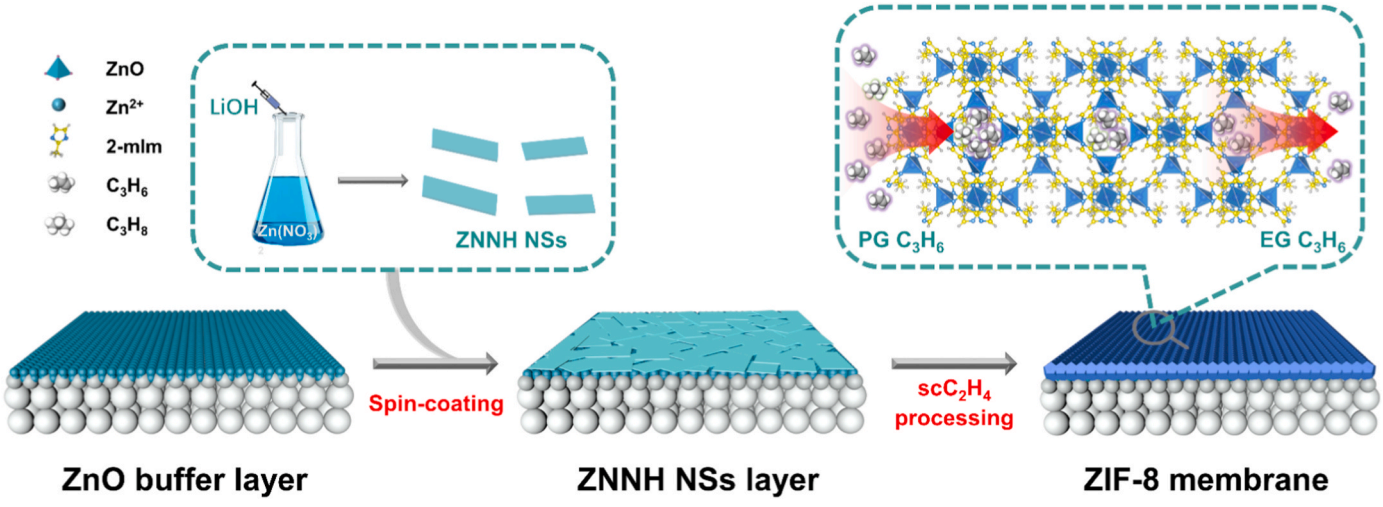


Fig. 1. Schematic illustration of the preparation of scC_2H_4-processed ZIF-8 membrane for EG C_3H_6 production.

supplied by Dalian Junfeng Gas Chemical Co., Ltd.

2.2. scC_2H_4 processing of ZIF-8 powders

ZIF-8 powders were prepared using scC_2H_4 as solvent. Specifically, 1 g of 2-mIm and 0.25 g of ZnO particles (molar ratio 2-mIm: ZnO = 4:1) were placed in a semi-permeable reactor. After vessel sealing, C_2H_4 was injected into the reaction system, and SCF processing was carried out under designated temperature and pressure. Upon completion of the reaction, C_2H_4 was vented, and residual ligands were recovered. Finally, obtained ZIF-8 powders were adequately rinsed with excess methanol and dried overnight at 70 °C before utilization.

2.3. Deposition of ZnO buffer layer

Porous α-Al_2O_3 supports underwent pretreatment in 6.0 wt% HCl aqueous solution. ZIF-8 nanocrystals (~70 nm) were synthesized as reported previously [48]. Afterwards, 0.01 g of above ZIF-8 nanocrystals were dispersed into 5 g methanol by ultrasonication and stirring to prepare a uniform suspension. Subsequently, 0.2 mL of seed suspension was spread on the substrate via spin-coating at 3000 rpm for 60 s. In the next step, Zn-based gel layer was coated over the seed layer following a previous study [49]. Finally, the deposited layer was transformed into ZnO buffer layer by calcination at 450 °C over 2 h, with a heating rate of 1 °C min^{-1}.

2.4. Deposition of ZNNH NSs layer

ZNNH NSs were prepared based on the procedure reported in the prior work [50]. Briefly, 5.95 g of $Zn(NO_3)_2{\cdot}6H_2O$ was dissolved in 100 mL of DI water, while 0.24 g of LiOH was dissolved in 50 mL of DI water. The LiOH solution was then added dropwise into the Zn $(NO_3)_2{\cdot}6H_2O$ solution at a rate of 15 mL h^{-1} under continuous stirring for 3 h. The acquired solid product was separated by vacuum filtration and dried to produce ZNNH NSs.

The ZNNH NSs layer was deposited on ZnO buffer layer through spin-coating: Initially, 0.015 g of ZNNH NSs were dispersed in 5 g of methanol via ultrasonication and stirring to prepare a monodispersed suspension. Afterwards, 0.3 mL of as-prepared suspension was spin-coated on the substrate at 3000 rpm for 60 s. This coating operation was repeated. Finally, the modified substrate was dried at 70 °C overnight.

2.5. Preparation ZIF-8 membrane via scC_2H_4 processing

Initially, 400 mg of 2-mIm ligands were grounded and placed at the bottom of the semipermeable reactor. Subsequently, the ZNNH NSs-modified substrate was fixed at the top of a semipermeable reactor. In the next step, the reactor was sealed and placed inside the supercritical reactor. After evacuation and repeated gas purging, C_2H_4 was charged into the system, followed by heating and pressurization to the specific reaction conditions for SCF processing. After the reaction, obtained ZIF-8 membrane was collected, immersed in methanol for 12 h, and eventually dried overnight at ambient temperature. Residual white powders were collected for characterization and recycling.

2.6. PDMS treatment of as-prepared ZIF-8 membrane

A PDMS layer was spin-coated on as-prepared ZIF-8 membrane [51]. Briefly, given amount of PDMS monomer and cross-linker (weight ratio = 10:1) were dissolved in n-heptane, followed by ultrasonication and stirring to obtain a 10 wt% PDMS coating solution. Subsequently, the PDMS layer was deposited onto as-prepared ZIF-8 membrane by spin-coating 0.2 mL of above solution at 3000 rpm for 60 s. Finally, the coated membrane was dried at 80 °C for 24 h.

3. Results and discussion

3.1. Preparation of ZIF-8 powders

We initially verified the feasibility of preparing ZIF-8 powders through scC_2H_4 processing. After placing 2-mIm ligands and ZnO powders in the reactor vessel, supercritical reaction was performed under given conditions. Based on the temperature (T) and pressure (P) involved, ZIF-8 powders were designated as ZIF-8$p_{T\text{-}P}$. SEM results revealed that both the morphology of as-synthesized ZIF-8 powders varied significantly under different synthetic conditions. Specifically, ZIF-8$p_{35\text{-}6}$ (Fig. 2a) exhibited irregular morphology with a mean size of ~70 nm. With increasing temperature and pressure, ZIF-8$p_{50\text{-}8}$ (Fig. 2b) showed enhanced interparticle fusion with slightly larger size of ~90 nm. In comparison, ZIF-8$p_{65\text{-}8}$ (Fig. 2c) achieved optimal morphology, displaying uniform, well-defined, and well-intergrown rhombic dodecahedra with an average size of ~150 nm. EDXS mapping (Fig. 2d) confirmed uniform distribution of Zn and C elements, confirming uniform elemental distribution for ZIF-8$p_{65\text{-}8}$. Further temperature elevation at constant pressure of 8 MPa resulted in the formation of ~170 nm-sized ZIF-8$p_{80\text{-}8}$ (Fig. 2e) and ~200 nm-sized ZIF-8$p_{95\text{-}8}$ (Fig. 2f), both of which exhibited irregular morphologies and comprised loosely stacked crystallites. To elucidate this phenomenon, ligand solubility measurements were conducted. Experimental results confirmed that excessively high temperature accelerated ligand dissolution at the expense of reduced crystallinity (Fig. S1). XRD patterns (Fig. 2g) verified that all synthesized powders belonged to pure ZIF-8 phase. To summarize, reaction temperature exerts a more dominant influence than reaction pressure on the size and crystallinity of as-prepared ZIF-8 particles in scC_2H_4 reaction media. In comparison, conducting the reaction at 65 °C and 8 MPa results in the formation of ZIF-8 powders with optimzed morphology.

TGA was further employed to evaluate thermal stability of as-synthesized ZIF-8 powders. As illustrated in Fig. 2h, all obtained ZIF-8 powders showed a decomposition temperature centering around 450 °C with ultimate weight loss highly dependent on synthetic conditions. The ZnO conversion ratio (CR) was calculated from TGA results following a previously reported method [35]. At 35 °C and 6 MPa, the ZnO CR was 15.2%, and increased remarkably to 82.0% upon increasing temperature and pressure to 95 °C and 8 MPa. Apparently, higher temperature and pressure facilitated ZIF-8 nucleation and growth, resulting in increased ZnO CR. It should be noted that the ZnO CR reached 32% after 24 h of reaction in scC_2H_4 at 65 °C and 8 MPa. This value was lower than those achieved via solvothermal route (95%) and in $scCO_2$ medium (95.2%), yet close to the conversion of 29.6% obtained in scC_2H_6 [35]. Such discrepancies should arise from the weak solvation capacity of neutral scC_2H_4. The inherent inertness in turn endows scC_2H_4 with unique advantage for precisely regulating the nucleation and growth kinetics of ZIF-8 particles.

In addition, the FT-IR spectrum of obtained ZIF-8 powders (Fig. S2) exhibited characteristic peaks at 421 $cm^{-1}$and 1580 cm^{-1}, assignable to Zn-N and C═N stretching vibrations, respectively. The bands in the range of 600-1400 cm^{-1} and 2900-3200 cm^{-1} correspond to vibrational modes of the imidazole ring and methyl groups of 2-mIm ligands, which further demonstrated that all synthesized particles corresponded to pure ZIF-8 phase. Notably, the intensities of above characteristic peaks steadily increased with increasing temperature and pressure, indicatively of enhanced crystallinity. Furthermore, textural properties of obtained ZIF-8 powders were quantified by N_2 adsorption-desorption analysis. As shown in Fig. 2i, all curves exhibit typical Type I isotherms, indicating intrinsic microporous nature of obtained ZIF-8 particles; upon increasing operation temperature and pressure, the BET surface area increased from 111.7 to 1153.9 m^2 g^{-1}, which was positively associated with the corresponding ZnO CR. In comparison, scC_2H_6-processed ZIF-8 powders yielded lower surface areas under comparable conditions [35]. Increased surface areas possibly caused by

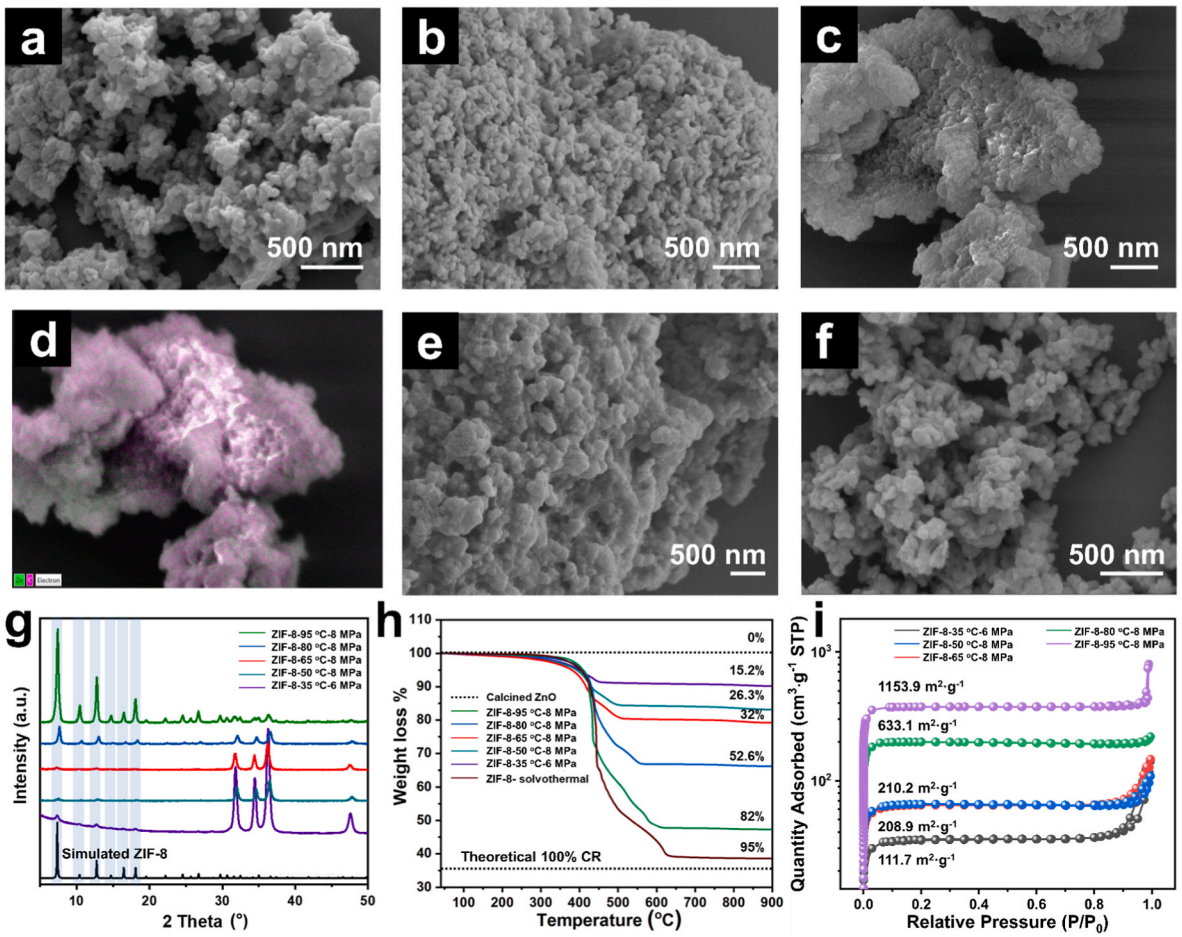


Fig. 2. Characterization of ZIF-8 powders prepared via scC_2H_4 processing under reaction conditions of (a) 35 °C and 6 MPa for 24 h, (b) 50 °C and 8 MPa for 24 h, (c) 65 °C and 8 MPa for 24 h, (d) EDXS image of ZIF-8 powders synthesized at 65 °C and 8 MPa for 24 h (Zn = green, C = pink), (e) 80 °C and 8 MPa for 24 h, and (f) 95 °C and 8 MPa for 24 h. (g) XRD patterns, (h) TGA curves, and (i) N_2 adsorption-desorption curves of ZIF-8 powders obtained under different conditions. (For interpretation of the references to colour in this figure legend, the reader is referred to the Web version of this article.)

enhanced crystallinity and reduced pore clogging are expected to provide abundant diffusion pathways for high-efficiency permeation of C_3H_6 in the membrane.

3.2. Preparation of ZIF-8 membranes

Aiming at suppressing excessive penetration and enhancing uniformity of ZnO buffer layer, prior to Zn-based sol spin-coating, a ZIF-8 crystal layer was deposited on the bare substrate. As shown in Fig. S3, ZIF-8 crystals were uniformly deposited on the substrate under optimized conditions. After spin-coating of Zn-based sol and the subsequent calcination, a smooth and uniform ZnO buffer layer was readily formed (Fig. S4). Corresponding XRD pattern verified that the resulting layer belonged to pure wurtzite-type ZnO (Fig. S5). Cross-sectional SEM image (Fig. S6) further demonstrated that ZnO buffer layer had partially infiltrated into substrate pores, which was conducive to improving the mechanical stability of as-prepared membrane.

Initially, we attempted to prepare qualified ZIF-8 membrane on ZnO buffer layer through in situ growth. However, it was proven to be challenging to prepare the membrane with well-defined morphology and satisfactory C_3H_6/C_3H_8 separation performance (Figs. S5 and S7, Table S1). Even under optimized reaction conditions (65 °C and 8 MPa), continuous ZIF-8 layer still could not be obtained, which may be attributed to the low nucleation density on the substrate [35].

To address this limitation, we tried to deposit a ZNNH NSs layer on ZnO buffer layer-modified substrate, considering that ZNNH NSs layer may exhibit higher reactivity and superior isolation effect than the ZnO buffer layer along. It is therefore expected that both higher C_3H_6 permeance and C_3H_6/C_3H_8 selectivity can be achieved through suppressed penetration of ligands into substrate pores and enhanced degree of intergrowth between adjacent crystallites [35,50]. As shown in Fig. S8, as-synthesized ZNNH NSs displayed uniform cubic morphology with an aspect ratio of ~60 and lateral size of ~8 μm, while relevant XRD pattern (Fig. 3l) verified its pure phase structure consistent with the literature [50]. ZNNH NSs were then deposited on ZnO buffer layer-modified substrate via spin-coating. Relevant SEM image (Fig. 3a) confirmed the formation of a smooth and continuous ZNNH layer, which was beneficial for microstructure optimization of ZIF-8 membranes. Therefore, the Zn-based buffer layer, which consisted of a bottom ZnO layer and a top ZNNH NSs layer, jointly served as zinc source of the ZIF-8 membrane. During the dissolution of reactive ZNNH NSs, sufficient ZIF-8 nucleation and growth at the substrate-solution interface were triggered, yielding the membrane with optimized interface structure; simultaneously, the high aspect ratio of ZNNH NSs facilitated their close packing to form ZIF-8 membrane with reduced grain-boundary defects. While a major function of the bottom ZnO layer was to strengthen interfacial adhesion between the substrate and as-prepared ZIF-8 layer [35,50]. Following the naming rule of powder samples, relevant membrane was designated as ZIF-8$m_{T\text{-}P(ISG)}$, where ISG denoted in situ growth in scC_2H_4 reaction medium.

Three sets of experiments were further performed to study the effects of temperature and pressure on the microstructure of ZIF-8 membranes.

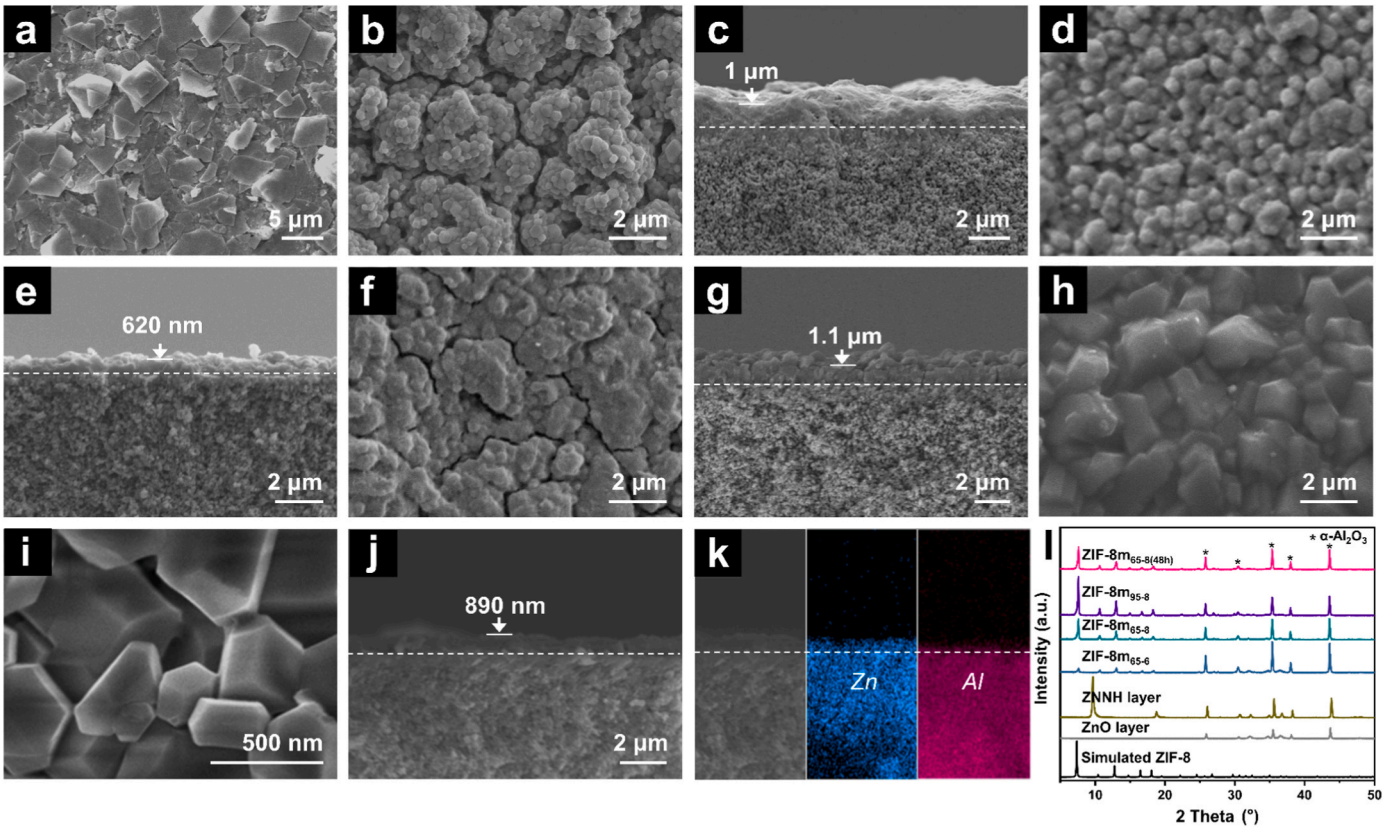


Fig. 3. (a) SEM image of ZNNH NSs layer, SEM images of (b, c) ZIF-8m$_{65\text{-}6(ISG)}$, (d, e) ZIF-8m$_{65\text{-}8(ISG)}$, (f, g) ZIF-8m$_{95\text{-}8(ISG)}$, and (h-j) ZIF-8m$_{65\text{-}8(ISG)}$ with reaction duration of 48 h. (k) EDXS mapping of ZIF-8 membrane synthesized at 65 °C and 8 MPa for 48 h (Zn = blue; Al = pink). (l) XRD patterns of simulated ZIF-8, ZnO buffer layer, ZNNH NSs layer, and ZIF-8 membranes synthesized under different reaction conditions. (For interpretation of the references to colour in this figure legend, the reader is referred to the Web version of this article.)

As shown in Fig. 3b, conduction reaction at 65 °C and 6 MPa resulted in the formation of ZIF-8m$_{65\text{-}6(ISG)}$ with severe particle agglomeration and clearly visible cracks on its surface, while cross-sectional SEM image showed that obtained layer was loosely attached to the substrate with a thickness of ~1.0 μm (Fig. 3c). In contrast, ZIF-8m$_{65\text{-}8(ISG)}$ (Fig. 3d) exhibited relatively smooth morphology with negligible intergranular gaps in the layer. Relevant cross-sectional image confirmed that its thickness reduced to ~620 nm with strong adhesion to the substrate (Fig. 3e). Nonetheless, further increasing the temperature to 95 °C caused excessive epitaxial growth, and therefore, granular agglomeration and crack generation in ZIF-8m$_{95\text{-}8(ISG)}$ (Fig. 3f); at the same time, the thickness reached ~1.1 μm (Fig. 3g). Therefore, carrying out the reaction at 65 °C and 8 MPa was considered optimum for obtaining ZIF-8 membranes with optimized microstructure. Notably, as evidenced by XRD patterns (Fig. 3l), no diffraction peaks assignable to ZNNH NSs could be discerned, indicating that the ZNNH NS buffer layer had been completely converted to due to the high chemical activity.

We further investigated the influence of reaction duration on membrane microstructure. As shown in Fig. 3h and i, extending the duration from 24 h to 48 h led to increased grain size (~770 nm) and thickness (~890 nm) accompanying with better intergrowth between neighboring crystallites. Cross-sectional EDXS mapping (Fig. 3k) further revealed that the top layer had partially penetrated into the substrate pores, resulting in enhanced mechanical stability. Relevant XRD pattern (Fig. 3l) verified that as-synthesized membrane belonged to pure ZIF-8 phase with higher crystallinity. Therefore, the optimum reaction duration was fixed to 48 h.

To further eliminate minor residual intergranular defects, prior to gas permeation test, as-synthesized ZIF-8 membrane was subjected to PDMS post-modification, which was commonly employed in defect healing of MOF membranes [51,52]. As illustrated in Figs. S9a, b, a thin PDMS layer (~300 nm) was uniformly covered the membrane surface with no obvious penetration into the substrate pores. It is therefore expected that the C_3H_6/C_3H_8 selectivity can be enhanced with negligible compromise in C_3H_6 permeance.

3.3. C_3H_6/C_3H_8 separation performance evaluation of ZIF-8 membranes

Finally, gas permeation properties of as-synthesized membranes were evaluated using a Wicke–Kallenbach cell (Fig. S10). As summarized in Table S2, ZIF-8m$_{65\text{-}6(ISG)}$ exhibited C_3H_6 permeance of 271.7×10^{-10} mol m^{-2} s^{-1}·Pa^{-1} with C_3H_6/C_3H_8 separation factor (SF) of 1.7. Upon increasing pressure to 8 MPa, both C_3H_6 permeance and C_3H_6/C_3H_8 SF of ZIF-8m$_{65\text{-}8(ISG)}$ increased to 758.4×10^{-10} mol m^{-2} s^{-1}·Pa^{-1} and 33.2, respectively. Nonetheless, further raising the temperature to 95 °C led to inferior C_3H_6 permeance (110.9×10^{-10} mol m^{-2} s^{-1}·Pa^{-1}) and C_3H_6/C_3H_8 SF (10.9) for ZIF-8m$_{95\text{-}8(ISG)}$. This is rational, since maintaining reaction condition at 65 °C and 8 MPa results in higher scC_2H_4 density (122.1 kg m^{-3}), rendering higher ligand solubility (Fig. S11), and therefore, sufficient nutrient supply during scC_2H_4 processing. In contrast, further lowering pressure to 6 MPa or increasing temperature to 95 °C leads to reduced scC_2H_4 density of 80.2 kg m^{-3} and 95.9 kg m^{-3}, respectively, causing lower ligand solubility, and therefore, grain boundary defect formation in the membrane.

Aiming at increasing C_3H_6/C_3H_8 SF further, we prolonged the reaction duration and conducted PDMS post-modification to seal intergranular defects in the membrane. The membrane obtained via supercritical reaction at 65 °C and 8 MPa for 48 h exhibited C_3H_6/C_3H_8 SF of 46.6 with C_3H_6 permeance of 454.5×10^{-10} mol m^{-2} s^{-1}·Pa^{-1}

(Table S2), while further conducting PDMS post-modification on 48 h-synthesized ZIF-8 membrane led to increased C_3H_6/C_3H_8 SF of 87.9 accompanied with only slight reduction in C_3H_6 permeance (202×10^{-10} mol m^{-2} s^{-1}·Pa^{-1}). To the best of our knowledge, our membrane exhibits superior C_3H_6 permeance among all reported supercritical-synthesized ZIF-8 membranes with no significant compromise in C_3H_6/C_3H_8 selectivity (Fig. 4a and Table S3).

Considering practical operation conditions and feedstock composition during EG C_3H_6 purification, the influence of operation temperature, operation pressure, and C_3H_6 feed concentration on the C_3H_6/C_3H_8 separation performance of our membrane was systematically investigated. As shown in Fig. 4b, upon increasing operation temperature from room temperature (RT) to 90 °C, the C_3H_6 permeance slightly increased (from 190.1×10^{-10} to 236.2×10^{-10} mol m^{-2} s^{-1}·Pa^{-1}), while the C_3H_8 permeance increased more pronouncedly (from 2.9×10^{-10} to 9.4×10^{-10} mol m^{-2} s^{-1}·Pa^{-1}), resulting in a notable decline in C_3H_6/C_3H_8 SF from 65 to 25 (Fig. 4b). Fortunately, the C_3H_6/C_3H_8 SF could be fully recovered upon decreasing the temperature to RT. To evaluate the industry-relevant low-temperature adaptability of our membrane, its separation performance was further evaluated from RT to −40 °C, the temperature adapted to EG C_3H_6 purification. Correspondingly, the permeance of C_3H_6 and C_3H_8 fell from 202×10^{-10} to 120.8×10^{-10} mol m^{-2} s^{-1}·Pa^{-1} and from 2.97×10^{-10} to 0.7×10^{-10} mol m^{-2} s^{-1}·Pa^{-1}, respectively. A greater extent of C_3H_8 permeance reduction caused prominent enhancement of C_3H_6/C_3H_8 SF to 174.9 at −40 °C. This is rational, since our recent research confirmed that reducing operation temperature suppressed the swing of framework ligands and boosted selective adsorption towards C_3H_6, jointly contributing to enhanced C_3H_6/C_3H_8 selectivity [16]. Cycling tests (Fig. 4b) further verified that C_3H_6/C_3H_8 separation performance could be fully recovered upon switching operation temperature from −40 °C to RT, demonstrating robust structure stability. Such reversible behavior validates its great potential in practical EG C_3H_6 production.

As reported in previous studies, the C_3H_6/C_3H_8 separation performance of ZIF-8 membranes commonly deteriorated upon increasing operation pressure, largely attributed to the presence of grain boundary defects in the membrane and/or enlarged pore size caused by framework deformation [53,54]. In contrast, our membrane only experienced limited reduction in C_3H_6 permeance (27.7%) and C_3H_6/C_3H_8 SF (23.7%) upon increasing pressure to 4 bar (Fig. 4c), far exceeding most

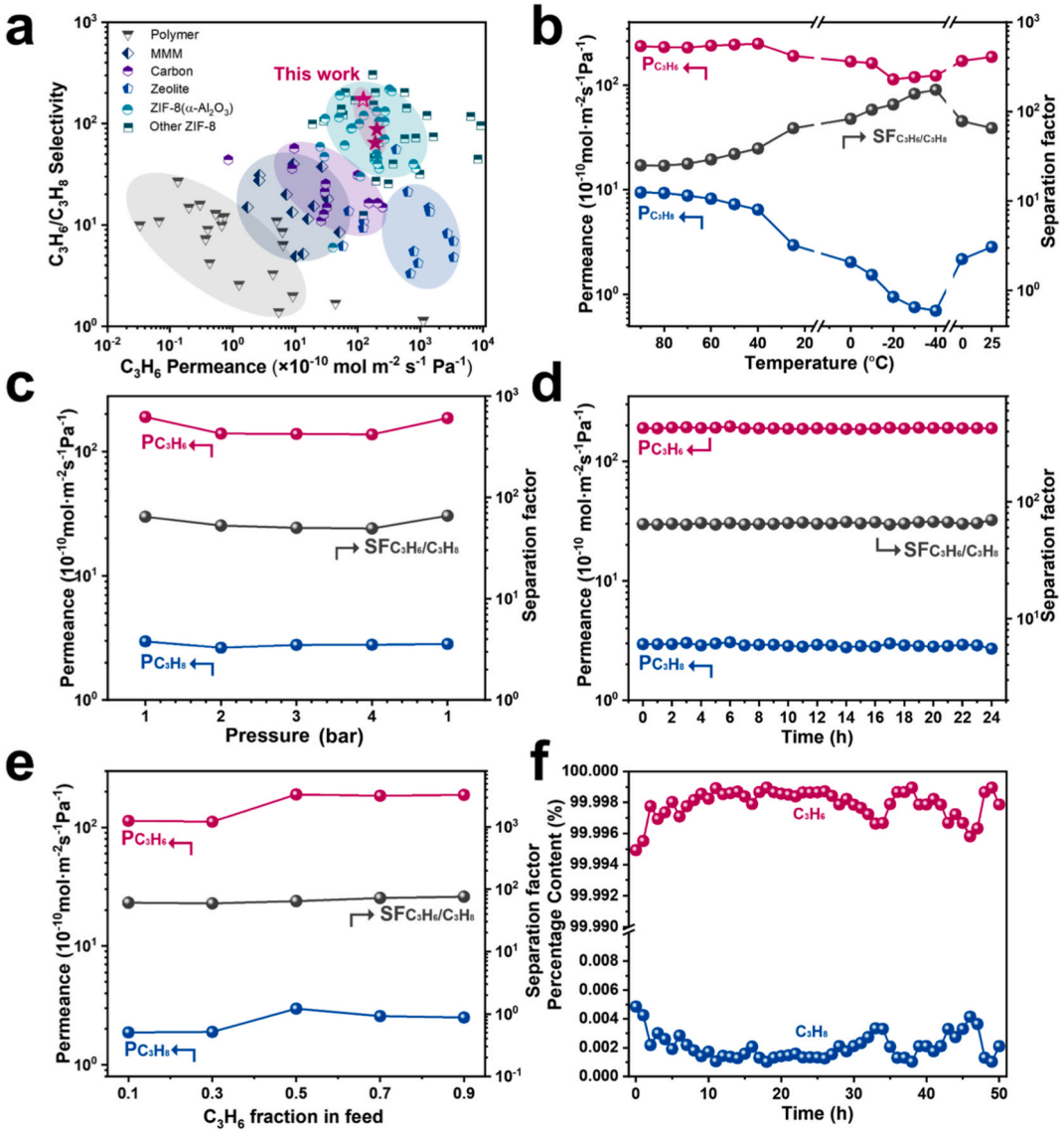


Fig. 4. (a) C_3H_6 permeance and C_3H_6/C_3H_8 SF of ZIF-8 membrane compared with previous literatures. The dependence of C_3H_6/C_3H_8 separation performance of ZIF-8 membrane on (b) operation temperature, (c) operation pressure, and (d) feed composition. (e) 24 h stability test of ZIF-8 membrane. (f) Long-term stability test of ZIF-8 membrane operated under −40 °C, 3 bar and vacuum conditions with polymer-grade C_3H_6 (~99.5%) as feedstock.

ZIF-8 membranes reported in the literature, which commonly experienced C_3H_6/C_3H_8 SF reduction ≥80% under pressurization [55,56]; moreover, its performance was completely reversible upon returning the operation pressure to atmospheric conditions. To further verify the durability of our membrane after low-temperature and pressurized operation, its long-term stability was evaluated. As displayed in Fig. 4d, both the C_3H_6 permeance (189.2×10^{-10} mol m^{-2} s^{-1}·Pa^{-1}) and C_3H_6/C_3H_8 SF (~65) remained largely unchanged during 24 h of continuous operation, demonstrating outstanding structural stability and operational reliability in terms of C_3H_6/C_3H_8 separation under ambient conditions.

Considering the extreme C_3H_6/C_3H_8 molar ratio in industry-relevant EG C_3H_6 production, the influence of feed composition on C_3H_6/C_3H_8 separation performance was investigated. As shown in Fig. 4e, as C_3H_6 molar ratio increased from 10% to 90%, the C_3H_6 permeance steadily increased from 113.6×10^{-10} to 188.6×10^{-10} mol m^{-2} s^{-1}·Pa^{-1}, in contrast, the C_3H_8 permeance remained 2.4×10^{-10} mol m^{-2} s^{-1}·Pa^{-1} throughout entire feed ratio range. As a result, its C_3H_6/C_3H_8 SF slightly increased from 60.8 to 75.8. In effect, such positive correlation between C_3H_6/C_3H_8 SF and C_3H_6 molar ratio has been rarely reported in previous studies, which commonly suffered SF decline upon increasing C_3H_6 fraction in the feed [35,55–58]. This can be attributed to the rigid framework and low-defect grain boundaries of ZIF-8 membranes under working conditions. Based on the above, as the C_3H_6 fraction in the feed increases, C_3H_6 partial pressure rises and modulates competitive adsorption in ZIF-8 pores, resulting in suppressed C_3H_8 diffusion and therefore, increased C_3H_6/C_3H_8 SF.

Aiming at industrial EG C_3H_6 production, we finally verified the capacity of our membrane to remove trace C_3H_8 under practical operation conditions with 99.5% PG C_3H_6 feed containing heavy impurities like C_3H_8, n-C_4H_{10} and i-C_4H_{10} (Table S4). Vacuum pumping was applied on the permeate side, while the operation temperature and pressure were kept at industrially relevant values of −40 °C and 3 bar, respectively. Gas permeation results revealed that our membrane delivered a C_3H_6/C_3H_8 SF of 169.5 with C_3H_6 flux of 3.6×10^{-3} mol m^{-2} s^{-1}. To the best of our knowledge, this represents the highest C_3H_6 flux among all membranes employed in EG C_3H_6 purification to date [16]; moreover, the C_3H_8 concentration in the permeate stream dropped sharply to below 50 ppm with n-C_4H_{10} and i-C_4H_{10} reduced to a level under the detection limit (Table S5). During a 50 h continuous test, the permeate-side C_3H_6 purity always surpassed 4 N (~99.994%) (Fig. 4f). The Above results demonstrate that our membrane enables high-efficiency purification of PG C_3H_6 into EG C_3H_6 in one step, providing a promising route to drastically save energy consumption and production cost with no compromise in EG C_3H_6 purity.

3.4. Sustainability of scC_2H_4 processing

After SCF processing, white solid powders recovered from the bottom of reactor was characterized. According to Fig. S12a and S12b, the morphological feature of residual solids matched that of raw 2-mIm ligands. Corresponding XRD pattern confirms that above powders still belong to pure 2-mIm phase (Fig. S12c). Furthermore, ATR-IR and XPS results reveal the no zinc-containing species are present within recovered powders (Fig. S12d and S12e), confirming that 2-mIm ligands can be fully recycled after scC_2H_4 processing. To verify their reusability, recovered 2-mIm ligands were utilized to synthesize ZIF-8 membranes. As shown in Fig. S12f, continuous and well-intergrown ZIF-8 membranes were successfully prepared, demonstrating intrinsic sustainability of scC_2H_4 reaction medium.

4. Conclusions

In this study, we pioneered a scC_2H_4-processed route for preparing C_3H_6-permselective ZIF-8 membranes for one-step EG C_3H_6 production from PG C_3H_6 feed. Relying on broader critical temperature-pressure window of scC_2H_4 and its reversible π-complexation with Zn^{2+} ions, both nucleation and growth kinetics of ZIF-8 crystallites on the substrate surface could be more accurately tailored; while pre-deposition of a ZNNH NSs buffer layer prior to scC_2H_4 processing further retarded nutrient penetration and promoted crystal intergrowth. Obtained membrane not only exhibited outstanding C_3H_6/C_3H_8 selectivity and C_3H_6 permeance under ambient conditions, but also could withstand varying operation conditions and feed composition. Such outstanding adaptability was confirmed under industrial refining conditions, delivering a C_3H_6/C_3H_8 SF of 169.5 and C_3H_6 flux of 3.6×10^{-3} mol m^{-2} s^{-1}. With PG C_3H_6 as feed gas, our membrane enabled one-step production of EG C_3H_6, reducing C_3H_8 below 50 ppm and fully eliminating C_4 heavy impurities. In addition, both unreacted 2-mIm ligands and vented C_2H_4 could be fully recovered, warranting zero-pollutant discharge during the whole process. Our study paves an avenue for sustainable preparation of high-flux MOF membranes towards high-efficiency production of high-purity electronic specialty gases.

CRediT authorship contribution statement

Wenjing Hu: Writing – original draft, Methodology, Investigation, Formal analysis, Data curation, Conceptualization. **Pengxiang Zhang:** Data curation. **Hua Jin:** Formal analysis. **Jiahui Yan:** Formal analysis. **Yuanchen Li:** Data curation. **Kunpeng Yu:** Formal analysis. **Weichong Wang:** Formal analysis. **Jiaxin Ma:** Formal analysis. **Yumei Meng:** Formal analysis. **Weijun Xu:** Formal analysis. **Kelin Dong:** Supervision, Funding acquisition, Conceptualization. **Yanshuo Li:** Supervision, Funding acquisition, Conceptualization. **Yi Liu:** Writing – review & editing, Writing – original draft, Supervision, Resources, Methodology, Funding acquisition, Conceptualization.

Declaration of competing interests

The authors declare that they have no known competing financial interests or personal relationships that could have appeared to influence the work reported in this paper.

Acknowledgements

The authors are grateful to National Key Research and Development Program of China (2023YFB3810700), National Natural Science Foundation of China (U22A20412), CNPC Youth Science and Technology Special Project (2026DQ03199), and Scientific Research and Technological Development Project of Dalian West Pacific Petrochemical Co., Ltd (26XTSHSG008) for the financial support.

Appendix A. Supplementary data

Supplementary data to this article can be found online at https://doi.org/10.1016/j.memsci.2026.126150.

Data availability

The authors do not have permission to share data.

References

[1] T. Ren, M. Patel, K. Blok, Olefins from conventional and heavy feedstocks: energy use in steam cracking and alternative processes, Energy 31 (2006) 425.
[2] D.S. Sholl, R.P. Lively, Seven chemical separations to change the world, Nature 532 (2016) 435–437.
[3] S. Yao, Y. Wang, B. Chen, L. Xu, H. Mao, Z. Zhao, Scalable large-area ZIF-8 membranes for industrial propylene/propane separations, Adv. Membr. 9 (2026) 100241.
[4] Z. Song, Y. Wang, Z. Zha, Z. Wang, S. Zhao, Porous organic cage separation membranes: exploratory journey from preparation to application, Adv. Membr. 5 (2025) 100125.

[5] S. Yao, Y. Wang, B. Chen, L. Xu, H. Mao, Z. Zhao, Fabrication of polymer-supported ZIF-8 membranes via interfacial-epitaxial coupled growth for C_3H_6/C_3H_8 separation, Adv. Membr. 9 (2026) 100241.

[6] T. Zhang, J.J. Lv, Y. Dang, Z. Gao, H. Wang, J.W. Cao, G.H. Zhang, H. Rao, F. P. Pan, K.J. Chen, High-throughput computational screening-driven porous material discovery for benchmark propylene/propane separation, Adv. Funct. Mater. 35 (2025) 2412457.

[7] Y. Wang, S.B. Peh, D. Zhao, Alternatives to cryogenic distillation: advanced porous materials in adsorptive light olefin/paraffin separations, Small 15 (2019) 1900058.

[8] D. Lee, S. Lee, I. Choi, M. Kim, Positional functionalizations of metal–organic frameworks through invasive ligand exchange and additory MOF-on-MOF strategies: a review, Smart Mol 2 (2024) e20240002.

[9] Y.F. Yuan, Y.S. Wang, X.L. Zhang, W.C. Li, G.P. Hao, L. Han, A.H. Lu, Wiggling mesopores kinetically amplify the adsorptive separation of propylene/propane, Angew. Chem. Int. Ed. 60 (2021) 19063–19067.

[10] X. Li, J. Yu, S. Han, Y. Zhou, Y. Liang, Y. Wang, Z. Wang, Ligand substitution engineering for modulating the pore microenvironment of MOFs to enhance CO_2 gas separation performance in mixed matrix membranes, Adv. Membr. 7 (2026) 100210.

[11] A. Harmens, Propylene-propane phase equilibrium from 230 to 350 K, J. Chem. Eng. Data 30 (1985) 230–233.

[12] M. Khalighi, Y.F. Chen, S. Farooq, I.A. Karimi, J.W. Jiang, Propylene/propane separation using SiCHA, Ind. Eng. Chem. Res. 52 (2013) 3877.

[13] Q. Ding, S. Zhang, Recent advances in the development of metal-organic frameworks for propylene and propane separation, Energ. Fuel. 36 (2022) 7337–7361.

[14] A. Cadiau, K. Adil, P.M. Bhatt, Y. Belmabkhout, M. Eddaoudi, A metal-organic framework-based splitter for separating propylene from propane, Science 353 (2016) 137–140.

[15] T. Xia, Y. Wu, T. Ji, W. Hu, K. Yu, X. He, B.H. Yin, Y. Liu, Mixed-matrix membranes incorporating hierarchical ZIF-8 towards enhanced CO_2/N_2 separation, Smart Mol 3 (2025) e20240066.

[16] K. Yu, Y. Dong, T. Ji, J. Liu, S. Gu, J. Yin, X. He, B. Zheng, J. Wang, Y. Gao, G. Maurin, Y. Liu, ZIF-8 membrane-based cryo-stripping of trace impurities towards electronic grade C_3H_6 production, Nat. Commun. 17 (2026) 6494.

[17] H. Ma, R. Wang, K. He, Y. Hu, G.P. Simon, H. Wang, Swelling polymer-regulated green synthesis of flexible ZIF-8 membrane, Adv. Membr. 5 (2025) 100144.

[18] K. Li, D.H. Olson, J. Seidel, T.J. Emge, H. Gong, H. Zeng, J. Li, Zeolitic imidazolate frameworks for kinetic separation of propane and propene, J. Am. Chem. Soc. 131 (2009) 10368–10369.

[19] H.T. Kwon, H.K. Jeong, A.S. Lee, H.S. An, J.S. Lee, Heteroepitaxially grown zeolitic imidazolate framework membranes with unprecedented C_3H_6/C_3H_8 separation performances, J. Am. Chem. Soc. 137 (2015) 12304–12311.

[20] S. Zhou, Y. Wei, L. Li, Y. Duan, Q. Hou, L. Zhang, L. Ding, J. Xue, H. Wang, J. Caro, Paralyzed membrane: current-driven synthesis of a metalorganic framework with sharpened propene/propane separation, Sci. Adv. 4 (2018) eaau1393.

[21] M.J. Lee, H.T. Kwon, H. Jeong, High-flux zeolitic imidazolate framework membranes for C_3H_6/C_3H_8 separation by postsynthetic linker exchange, Angew. Chem. Int. Ed. 57 (2018) 156–161.

[22] Y.C. Pan, T. Li, G. Lestari, Z.P. Lai, Effective separation of C_3H_6/C_3H_8 binary mixtures by ZIF-8 membranes, J. Membr. Sci. 390 (2012) 93–98.

[23] Q. Ma, X. Wang, H. Jin, S.W. Feng, W. Fang, Y.S. Li, Highly permeable ZIF-8 membranes for propylene permselective pervaporation under high pressure up to 20 bar, J. Membr. Sci. 643 (2022) 120055.

[24] D.I. Kolokolov, A.G. Stepanov, H. Jobic, Mobility of the 2-Methylimidazolate linkers in ZIF-8 probed by 2H NMR: Saloon doors for the guests, J. Phys. Chem. C 119 (2015) 27512–27520.

[25] S.A. Moggach, T.D. Bennett, A.K. Cheetham, The effect of pressure on ZIF-8: increasing pore size with pressure and the formation of a high-pressure phase at 1.47 GPa, Angew. Chem. Int. Ed. 11 (2009) 7221–7223.

[26] T. Ji, L. Liu, Y. Sun, Y. Liu, G. Xu, J. Yan, G. He, Y. Liu, Sub-zero temperature synthesis of pressure-resistant ZIF-8 membrane with superior C_3H_6/C_3H_8 separation performance, ACS Mater. Lett. 4 (2022) 1094–1100.

[27] K. Eum, C. Ma, A. Rownaghi, C.W. Jones, S. Nair, ZIF-8 membranes via interfacial microfluidic processing in polymeric hollow fibers: efficient propylene separation at elevated pressures, ACS Appl. Mater. Interfaces 8 (2016) 25337–25342.

[28] Y. Gu, J. Hua, J. Chen, W. Zhu, R. Hou, C. Wang, Y. Pan, Rigid-interface-locking of ZIF-8 membranes to enable for superior high-pressure propylene/propane separation, J. Membr. Sci. 668 (2023) 121193.

[29] Q. Zhao, M. Zhao, W. Wang, Z. Song, J. Wang, Y. Tian, Q. Pan, H. Ma, S. Yuan, S. Guo, Y. Yang, Y. Li, R. Zhou, G. He, Z. Jiang, Nanosheet-bridged metal-organic framework membranes for durable hydrocarbon separation under high pressure, Sci. Adv. 11 (2025) eadz3219.

[30] X. Ma, P. Kumar, N. Mittal, A. Khlyustova, P. Daoutidis, K.A. Mkhoyan, M. Tsapatsis, Zeolitic imidazolate framework membranes made by ligand-induced permselectivation, Science 361 (2018) 1008–1011.

[31] Q. Ma, K. Mo, S. Gao, Y. Xie, J. Wang, H. Jin, A. Feldhoff, S. Xu, J. Lin, Y. Li, Ultrafast semi-solid processing of highly durable ZIF-8 membranes for propylene/propane separation, Angew. Chem. Int. Ed. 59 (2020) 21909–21914.

[32] Z. Zhang, H. Zhu, H. Jin, Y. Cao, W. Fang, Z. Zhang, Q. Ma, J. Choi, Y. Li, Restricting linker rotation in nanocages of ZIF-8 membranes using crown ether "Molecular Locks" for enhanced propylene/propane separation, Angew. Chem. Int. Ed. 63 (2024) e202415023.

[33] J. Wang, W. Bai, Y. Gao, Y. Ying, D. Liu, Q. Yang, Pressure-resistant propylene/propane separation by ZIF-8 membranes decorated with polyether-block-amide copolymer, AIChE J. 72 (2026) e70473.

[34] Q. Ma, X. Wang, H. Jin, S. Feng, W. Fang, Y. Li, Highly permeable ZIF-8 membranes for propylene permselective pervaporation under high pressure up to 20 bar, J. Membr. Sci. 643 (2022) 120055.

[35] K. Yu, T. Ji, M. Wu, S. Chen, Y. Gao, J. Yan, S. Meng, W. Hu, X. Fan, W. Dong, J. Yin, Y. Liu, Supercritical ethane processing of ZIF-8 membranes towards pressure-resistant C_3H_6/C_3H_8 separation, Angew. Chem. Int. Ed. 64 (2025) e202422709.

[36] C.A. Eckert, B.L. Knutson, P.G. Debenedetti, Supercritical fluids as solvents for chemical and materials processing, Nature 383 (1996) 313–318.

[37] A. Lopez-Periago, O. Vallcorba, C. Frontera, C. Domingo, J.A. Ayllon, Exploring a novel preparation method of 1D metal organic frameworks based on supercritical CO_2, Dalton Trans 44 (2015) 7548–7553.

[38] J.M. Marrett, C. Mottillo, S. Girard, C.W. Nickels, J.L. Do, G. Dayaker, L. S. Germann, R.E. Dinnebier, A.J. Howarth, O.K. Farha, T. Friscic, C.J. Li, Supercritical carbon dioxide enables rapid, clean, and scalable conversion of a metal oxide into zeolitic metal-organic frameworks, Cryst. Growth Des. 18 (2018) 3222–3228.

[39] L. Liu, Y. Song, T. Ji, Y. Sun, D. He, H. Hu, Y. Liu, Beyond solution-based protocols: MOF membrane synthesis in supercritical environments for an elegant sustainability performance balance, ACS Mater. Lett. 2 (2020) 1142–1147.

[40] M.A. Sinnwell, Q.R.S. Miller, L. Liu, J. Tao, M.E. Bowden, L. Kovarik, D. Barpaga, Y. Han, R. Kishan Motkuri, M.L. Sushko, H.T. Schaef, P.K. Thallapally, Kinetics and mechanisms of ZnO to ZIF-8 transformations in supercritical CO_2 revealed by in situ X-ray diffraction, ChemSusChem 13 (2020) 2602–2612.

[41] L. Liu, T. Ji, W. Hu, Y. Sun, Y. He, J. Yan, G. He, Y. Liu, Epitaxial supercritical fluid processing of ZIF-8 membranes towards efficient C_3H_6/C_3H_8 separation, J. Membr. Sci. 669 (2023) 121300.

[42] L. Liu, W. Hu, Y. Sun, T. Ji, Y. He, K. Yu, M. Wu, G. He, Y. Liu, Coupling atomic layer deposition with supercritical fluid processing to provide a highly C_3H_6-selective ZIF-8 membrane, AIChE J. 70 (2024) 18385.

[43] R.V. Shende, S.J. Lombardo, Supercritical extraction with carbon dioxide and ethylene of poly(vinyl butyral) and dioctyl phthalate from multilayer ceramic capacitors, J. of Supercritical Fluids 23 (2002) 153–162.

[44] A. Capuzzo, M.E. Maffei, A. Occhipinti, Supercritical fluid extraction of plant flavors and fragrances, Molecules 18 (2013) 7194–7238.

[45] A. Wooten, P.J. Carroll, A.G. Maestri, P.J. Walsh, Unprecedented alkene complex of Zinc(II): structures and bonding of divinylzinc complexes, J. Am. Chem. Soc. 128 (2006) 4624–4631.

[46] C. Mottillo, T. Friščić, Carbon dioxide sensitivity of zeolitic imidazolate frameworks, Angew. Chem. Int. Ed. 53 (2014) 7471–7474.

[47] Z.N. Lashchinskaya, A.A. Gabrienko, S.S. Arzumanov, A.A. Kolganov, A. V. Toktarev, D. Freude, J. Haase, A.G. Stepanov, Which species, Zn^{2+} cations or ZnO clusters, are more efficient for olefin aromatization? ^{13}C Solid-Statsolid-snvestigation of n-But-1-ene Transformation on Zn-Modified Zeolite, ACS Catal. 10 (2020) 14224–14233.

[48] J. Cravillon, R. Nayuk, S. Springer, A. Feldhoff, K. Huber, M. Wiebcke, Controlling zeolitic imidazolate framework nano- and microcrystal formation: insight into crystal growth by time-resolved in situ static light scattering, Chem. Mater. 23 (2011) 2130–2141.

[49] X. Sun, Y. Qi, X. Che, L. Zhou, Y. Li, L. Zhang, J. Hu, A general and green approach of pH-sensitive ZIF-67 for encapsulating active substances, smart, Mol 4 (2026) e70040.

[50] O. Kwon, M. Kim, E. Choi, J. Bae, S. Yoo, J. Won, Y. Kim, J. Shin, J. Lee, D. Kim, High-aspect ratio zeolitic imidazolate framework (ZIF) nanoplates for hydrocarbon separation membranes, Sci. Adv. 8 (2022) eabl6841.

[51] L. Wu, J. Hua, Y. Gu, J. Sun, Q. Wang, L. Zhang, H. Lian, Y. Pan, In-situ cross-linking and shear-driven coating enable defect-free tubular ZIF-8 membranes toward efficient C_3H_6/C_3H_8 separation, J. Membr. Sci. 725 (2025) 124010.

[52] L. Sheng, C. Wang, F. Yang, L. Xiang, X. Huang, J. Yu, L. Zhang, Y. Pan, Y. Li, Enhanced C_3H_6/C_3H_8 separation performance on MOF membranes through blocking defects and hindering framework flexibility by silicone rubber coating, Chem Commun 53 (2017) 7760–7763.

[53] H. Lian, J. Hua, Q. Wang, E. Song, Y. Gu, Y. Pan, W. Xing, Scalable large-area ZIF-8 membranes for industrial C_3H_6/C_3H_8 separations, Nat. Chem. Eng. 3 (2026) 223–233.

[54] D. Li, M. Ye, C. Ma, N. Li, Z. Gu, Z. Qiao, Preparation of a self-supported zeolite glass composite membrane for CO_2/CH_4 separation, Smart Mol 2 (2024) e20240009O.

[55] T. Ji, L. Liu, M. Wu, K. Yu, X. He, Y. Liu, Subfreezing conversion of ALD-derived ZnO layer to ultra-thin ZIF-8 membrane for high-flux C_3H_6 production, Chem. Eng. Sci. 282 (2023) 119293.

[56] T. Ji, J.H. Yan, Y.F. He, W.J. Hu, Y. Peng, W.S. Yang, Y. Liu, Towards ZIF-8 membranes with superb C_3H_6/C_3H_8 separation performances under varying conditions: necessity of precise temperature control, J. Membr. Sci. 683 (2023) 121776.

[57] L. Liu, T. Ji, W. Hu, Y. Sun, Y. He, J. Yan, G. He, Yi Liu, Epitaxial supercritical fluid processing of ZIF-8 membranes towards efficient C_3H_6/C_3H_8 separation, J. Membr. Sci. 669 (2023) 121300.

[58] Q. Ma, K. Mo, S. Gao, Y. Xie, J. Wang, H. Jin, A. Feldhoff, S. Xu, J.Y.S. Lin, Y. Li, Ultrafast semi-solid processing of highly durable ZIF-8 membranes for C_3H_6/C_3H_8 separation, Angew. Chem. Int. Ed. 59 (2020) 21909.